MEDICAL SCIENCE MONITOR

DIAGNOSTIC TECHNIQUES

e-ISSN 1643-3750
© Med Sci Monit, 2019; 25: 2195-2205
DOI: 10.12659/MSM.913243

Received: 2018.09.17
Accepted: 2018.11.21
Published: 2019.03.25

Use of an Anthropomorphic Chest Model to Evaluate Multiple Scanning Protocols for High-Definition and Standard-Definition Computed Tomography to Detect Small Pulmonary Nodules

Authors' Contribution:
Study Design A
Data Collection B
Statistical Analysis C
Data Interpretation D
Manuscript Preparation E
Literature Search F
Funds Collection G

ABCDEF Liang Jin
BC Yingli Sun
DEFG Ming Li

Department of Radiology, Huadong Hospital, Affiliated to Fudan University, Shanghai, P.R. China

Corresponding Author: Ming Li, e-mail: minli77@163.com
Source of support: This study received funding from the Shanghai Shenkang Development Center (SHDC22015025) and the National Key R&D Program of China (2017YFC011905)

Background: This study aimed to use the LUNGMAN N1 anthropomorphic chest model to evaluate protocols for high-definition computed tomography (HDCT) and standard-definition CT (SDCT) to detect and compare small pulmonary nodules and determine the most appropriate low-dose scanning protocols.

Material/Methods: HDCT imaging used the Discovery HD750 scanner (80, 100, 120 and 140 kVp; 360, 320, 280, 240, 200, 160, 120, 80, 40, and 20 mA), and SDCT imaging used the Lightspeed VCT scanner (80, 120, and 140 kVp; 360, 320, 280, 240, 200, 160, 120, 80, 40, and 20 mA). The LUNGMAN N1 anthropomorphic chest model contained artificial pulmonary nodules (diameter: 5, 8, 10, and 12 mm). Low-dose scanning protocols were used in image acquisition. Two experienced radiologists evaluated the image quality. The combinations of voltage, tube current, image noise, and radiation dose were recorded. Consistency of the image quality between raters was assessed by kappa statistical analysis.

Results: Seventy CT scans of pulmonary nodules (diameter, 5–12 mm) were performed. There was a high degree of consistency for image quality between the two observers (K=0.929 for 5 mm nodules; K=0.819 for overall image quality). For 8 mm nodules, 100% were detected on both SDCT and HDCT. HDCT outperformed SDCT by 5%, in terms of effective dose. There was no significant difference in image quality between the SDCT and HDCT scanners.

Conclusions: Using an anthropomorphic chest model, the identification and image quality using SDCT was similar to that of HDCT for small pulmonary nodules between 5–12 mm.

MeSH Keywords: Multiple Pulmonary Nodules • Radiation Dosage • Tomography Scanners, X-Ray Computed

Full-text PDF: https://www.medscimonit.com/abstract/index/idArt/913243

Indexed in: [Current Contents/Clinical Medicine] [SCI Expanded] [ISI Alerting System] [ISI Journals Master List] [Index Medicus/MEDLINE] [EMBASE/Excerpta Medica] [Chemical Abstracts/CAS]

Background

Worldwide, lung cancer remains the leading cause of cancer deaths [1]. Lung cancer is often diagnosed at a late stage when patients may not respond to treatment. Therefore, there has been increasing interest in screening for lung cancer using computed tomography (CT) imaging to detect the lung cancer at an early stage [2,3].

Guidelines for the diagnosis of pulmonary nodules and patient follow-up, published by the Fleischner Society in 2017, indicate that regular follow-up is not essential for patients with pulmonary nodules that are low-risk (<6 mm) [4]. However, from 2010 in our hospital, many of the lung nodules measuring <10 mm have been diagnosed histologically as early-stage lung cancer, and these cases have included a large proportion of lung nodules measuring <6 mm in diameter [3]. Therefore, the identification and diagnosis of lung cancer nodules <10 mm in diameter remain an important clinical challenge [4].

Currently, the use of imaging with pulmonary CT scans is recognized as a diagnostic method to improve the survival rate and quality of life for patients with lung cancer [4,5]. As pulmonary CT scans are widely used, the radiation dose may be a concern. Some studies have shown that although the effect of a single radiation dose of routine CT imaging can be negligible, a single high-dose CT and cumulative radiation can be potentially carcinogenic [5-7]. Several published studies have described the potential of low-dose CT imaging in identifying lung nodules with a small diameter and volume, and with accuracy. However, the establishment of lung cancer screening programs using CT imaging has been limited by screening conditions, including scanning devices, scanning modes, and scanning parameters, and the lack of imaging algorithms, and so the selection of the appropriate parameters for pulmonary CT scanning present an important challenge for radiologists [8–11].

Recent reports have shown that many small pulmonary nodules, or ground-glass opacity nodules (GGNs), <5 mm in diameter can be diagnosed histologically as lung cancer [12,13]. With the development of CT scanners, low-dose CT (LDCT) scanning protocols have been applied to lung cancer screening, but not all CT scanners are not suitable for use in screening. The present study used the 2017 Fleischner guidelines to examine lung nodules >5 mm, and lung nodules <10 mm [4].

This study aimed to use the LUNGMAN N1 anthropomorphic chest model to evaluate protocols for high-definition computed tomography (HDCT) and standard-definition CT (SDCT) to detect small pulmonary nodules and to determine the most appropriate low-dose scanning protocols.

Material and Methods

Materials

The LUNGMAN N1 phantom multi-purpose anthropomorphic chest model (size, 43×40×48 cm, weight 18 kg, and chest circumference 94 cm) designed by Kyoto Kagaku (Kyoto, Japan) was used (Figure 1). The phantom is an accurate life-sized anthropomorphic model of a healthy male thorax. The rates of X-ray absorption of soft tissues and bone are similar to those of human tissues. The internal structures were removable, including the pulmonary vessels, trachea, heart, mediastinum, and some abdominal structures. These models can be used for chest X-ray and computed tomography (CT) scan studies, as the models closely resemble the human chest.

In the LUNGMAN N1 model, two kinds of lung nodules were used, one with a density of –630 Hounsfield units (HU) and diameters of 5, 8, 10, and 12 mm, and another with a density of –800 HU and diameters of 5, 8, 10, and 12 mm. A total of eight nodules were randomly placed in the anthropomorphic chest model (Figures 2, 3). These nodules have been previously used by other researchers to study ground-glass opacity nodules (GGNs), and it has been reported in the literature that the CT values of these nodules are similar to those of GGNS [14–16].

Image acquisition

The scanning range of the anthropomorphic chest model was performed from the lung apex to the lung base. The initial scanning position was marked to ensure the consistency in terms of length and range in each scan. Standard-definition CT (SDCT) and high-definition CT (HDCT) were used in image acquisition.

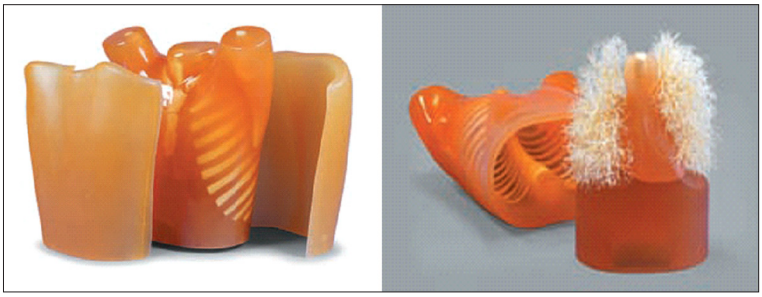

Figure 1. The LUNGMAN N1 phantom multipurpose anthropomorphic chest model.

Indexed in: [Current Contents/Clinical Medicine] [SCI Expanded] [ISI Alerting System] [ISI Journals Master List] [Index Medicus/MEDLINE] [EMBASE/Excerpta Medica] [Chemical Abstracts/CAS]

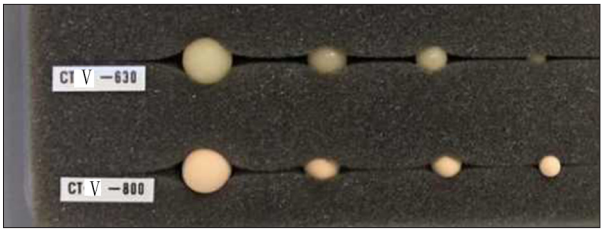

Figure 2. Eight spherical nodules with four diameters (5, 8, 10, and 12 mm) and two densities.

The anthropomorphic chest model was scanned multiple times using SDCT and the Lightspeed VCT (GE Healthcare, Waukesha, WI, USA). The tube voltages were set at 80, 120, and 140 kVp, with tube currents being set at 360, 320, 280, 240, 200, 160, 120, 80, 40, and 20 mA. The specification of slice thickness and slice interval each were 5 mm each. The display field of view (DFOV) was 40 cm, the scanning field of view (SFOV) was 50 cm, the spiral pitch was 0.984, and the rotation time was 0.5 s/rot. As SDCT lacked an adaptive statistical iterative reconstruction algorithm (ASIR), a set of filtered back projection (FBP) images with slice thickness and slice interval each of 0.625 mm each, along with a bone reconstruction algorithm (window width of 1500 HU and window level of -500 HU) were reconstructed after screening. Also, a set of FBP images with slice thickness and slice interval of 0.625 mm each and soft tissue window by standard reconstruction (window width of 350 HU and window level of 50 HU) were also reconstructed (Table 1).

The Discovery HD750 HDCT scanner was used (GE Healthcare, Waukesha, WI, USA). The tube voltages were set to 80, 100, 120, and 140 kVp, whereas the tube currents were set to 360, 320, 280, 240, 200, 160, 120, 80, 40, and 20 mA. The slice thickness and slice interval of the scanning were set at 5 mm each for scanning. However, the display field of view (DFOV) was 40 cm, the scanning field of view (SFOV) was 50 cm, the spiral pitch was 0.984, and the rotate time 0.5 s/rot. On scanning, a set of images with adaptive statistical iteration reconstruction (ASIR),

Simulated tumors
Size: diameter 3, 5, 8, 10, 12mm
Shape: sphere

	Color	Hounsfield number	Material
A	Cream	Approx. HU+100	Polyurethane. SZ50 and hydroxyapatie
B	White	Approx. HU-800	Urethane foam
C	Pale orange	Approx. HU-630	Urethane foam

Total 15 piece

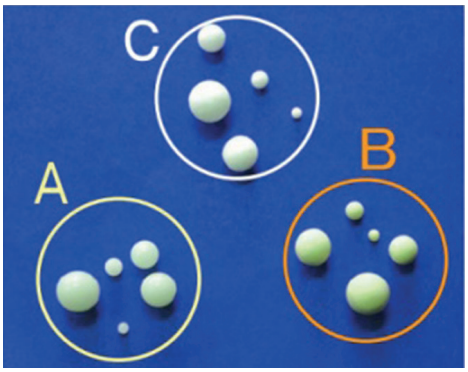

Figure 3. Introduction of the chest model nodules using the LUNGMAN N1 phantom multipurpose anthropomorphic chest model.

with 40% weighted ASIR was used, which is a recommended level for ASIR, according to previous studies [17–20]. A slice thickness and slice interval of 0.625 mm was applied, using a bone reconstruction algorithm, with a window width of 1500 HU and window level of –500 HU, and a set of images with 40% weighted ASIR, slice thickness of 0.625 mm, slice interval of 0.625 mm, as well as standard reconstruction algorithm, with a window width of 350 HU and a window level of 50 HU, were reconstructed. All the images were processed using the image processing station, ADW4.4 (GE Healthcare, Waukesha, WI, USA).

Table 1. Scanning parameters.

Devices	Discovery HD750(HDCT)				Lightspeed VCT(VCT)		
Tube voltage (kVp)	80	100	120	140	80	120	140
Tube current (mA)	360, 320, 280, 240, 200, 160, 120, 80, 40, 20				360, 320, 280, 240, 200, 160, 120, 80, 40, 20		
Reconstruction series 1	ASiR 40% + bone reconstruction algorithm, window width 1 500 HU, window level 500 HU, slice thickness of 0.625 mm and interval of 0.625 mm				FBP + bone reconstruction algorithm, window width 1500 HU, window level –500 HU, slice thickness of 0.625 mm, and interval of 0.625 mm		
Reconstruction series 2	ASiR 40% + stand reconstruction algorithm, window width 350 HU, window level 50 HU, slice thickness of 0.625 mm and interval of 0.625 mm				FBP + stand reconstruction algorithm, window width 350 HU, window level 50 HU, slice thickness of 0.625 mm, and interval of 0.625 mm		

Indexed in: [Current Contents/Clinical Medicine] [SCI Expanded] [ISI Alerting System] [ISI Journals Master List] [Index Medicus/MEDLINE] [EMBASE/Excerpta Medica] [Chemical Abstracts/CAS]

Measurement data

Two senior pulmonary radiologists measured CT values and image noise of the eight spherical pulmonary nodules. The region of interest (ROI) was set at 1 mm^2, given that the pulmonary nodules were 5 mm, which implied that the impact of the excessive volume effect could be overcome if the ROI was 1 mm^2, while measuring the CT values of the pulmonary nodules. The ROI was imaging slice was through the center of the pulmonary nodules. The standard deviation of the air-CT value, 3 cm above the sternal angle was set as the image noise, with the ROI being 200 mm^2. All the ROIs were placed in a similar manner, using a copy and paste function, to ensure the consistency of their respective position and size. Data represented the mean values of the measurements taken in triplicate.

Image analysis and evaluation

For all images, a double-blind evaluation was performed by two radiologists, each with more than 15 years of experience in chest imaging diagnosis. The overall image noise and the detection ability of the pulmonary nodules were assessed.

The radiologists also evaluated the image quality and display of the lesions on each image. All the images were scored based on the 5-point scale as follows: 1, unacceptable; 2, barely acceptable; 3, acceptable; 4, good; 5, perfect. The display of lesions was also scored according to the 5-point scale as follows: 1, the lesion could not be identified due to artifact; 2, the lesion may be non-existent and due to artifact; 3, the microstructure of the lesion could be displayed without artifact; 4, the lesion and its boundary was discernible; 5, the lesion and its boundary were displayed clearly. The results obtained from the two radiologists were analyzed statistically.

Radiation dose

The dose length product (DLP) parameters were generated automatically on the devices and were recorded. The DLP values were multiplied by K (conversion factor) to obtain the effective dose (effective dose=DLP×K), and the K value was set to 0.014.

Statistical analysis

Statistical analysis was performed using SPSS version 22.0 software (IBM, Chicago, IL, USA). The measured pulmonary nodules and air-CT values were compared using the one-sample t-test. Group-wise comparison of image noise was performed by analysis of variance (ANOVA). The CT values of SDCT and HDCT imaging datasets were compared using the Wilcoxon signed rank test. The consistency of the image quality was assessed by kappa analysis. $P<0.05$ was considered to be statistically significant.

Results

Evaluation of image quality

The differences in air-CT detected under various scanning conditions were not statistically significant ($P=0.380$). The image noise showed a significantly increasing trend with the decrease in the current ($P<0.05$). The image noise did not alter significantly with the changes in the tube voltage, with a fixed tube current on the Discovery HD750 scanner and fixed tube current on the Lightspeed VCT scanner. The P-values for image noise and tube voltage, obtained by univariate analysis, were 0.055 and 0.882, respectively. The CT values of nodules (5 mm, 100 HU; 5 mm, –630 HU; 5 mm, –800 HU), muscle, descending aorta, and air measured by the Lightspeed VCT scanner and the Discovery HD750 scanner at 80 kV, 120 kV, and 140 kV were compared (Table 2). Significant differences were observed in the CT values of nodules, muscle, descending aorta, and air ($P=0.039$, $P=0.033$, $P=0.018$, and $P=0.020$).

Detection of image quality, pulmonary nodules, and evaluation of detection criteria

The two radiologists achieved high consistency in the assessment of image quality of the pulmonary nodules (K=0.819) (Table 3) and showed high consistency of the detection criteria of the pulmonary nodules (K=0.929) (Table 3).

The detection of pulmonary nodules with a diameter of ≥5 mm and density ≥–630 HU were performed using high-definition computed tomography (HDCT) and standard-definition CT (SDCT). On HDCT, all pulmonary nodules could be detected via the scanning parameters as follows: 140 kVp and 20 mA, 120 kVp and 20 mA, 100 kVp and 20 mA, along with 80 kVp and 40 mA, and the effective dose (ED) was the lowest (0.38 mSv) at 100 kVp and 20 mA. The detection requirements of all the pulmonary nodules could be achieved at the scanning parameters as follows: 140 kVp and 20 mA, 120 kVp and 40 mA, 100 kVp, and 80 mA, along with 80 kVp and 80 mA, while the ED was the lowest (0.81 mSv) at 8 0kVp and 80 mA.

On SDCT, all the pulmonary nodules could be detected via the scanning parameters as follows: 140 kVp and 20 mA, 120 kVp and 20 mA, as well as 80 kVp, and 40 mA, while the ED was the lowest (0.40 mSv) at 80 kVp and 40 mA. The detection requirements of all pulmonary nodules could be achieved at the following scanning parameters: 140 kVp and 40 mA, 120 kVp and 80 mA, along with 80 kVp and 120 mA, and the ED was the lowest (1.20 mSv) at 80 kVp and 120 mA (Tables 4, 5 and Figures 4, 5).

The detection of pulmonary nodules with diameter ≥5 mm and density ≥–800 HU on HDCT showed that all pulmonary

Indexed in: [Current Contents/Clinical Medicine] [SCI Expanded] [ISI Alerting System] [ISI Journals Master List] [Index Medicus/MEDLINE] [EMBASE/Excerpta Medica] [Chemical Abstracts/CAS]

Table 2. Comparison of CT value of VCT and HDCT image data.

5 mm, 100 HU		5 mm, –630 HU		5 mm, –800 HU		Muscle		Descending aorta		Air	
HDCT	VCT	HDCT	VCT	HDCT	VCT	HDCT	VCT	HDCT	VCT	HDCT	VCT
135.33	181.33	–618.50	–570.17	–771.50	–33794	–19.33	6.33	5.75	49.89	–999.33	–971
128.78	192.78	–634.75	–665	–760.67	–33794	–16.00	–186.33	47.75	–50.56	–1001.33	–961.5
118.56	178	–625.00	–763.67	–815.11	92.33	–40.33	53.22	23.50	–995.17	–998.27	259
110.56	190	–652.00	–632	–771.17	–767.67	–8.50	–83.89	20.00	16.44	–998.47	–1006.17
127.67	133.89	–629.25	–600.5	–770.17	–771.33	–27.67	–48	22.25	15.11	–1002.93	–996.11
134.44	118	–661.50	–630.33	–764.00	738.83	–10.83	–56.67	49.50	40.56	–997.13	–1007
133.22	110.83	–608.25	–641.89	–772.50	–748.5	–7.33	–44.44	25.50	4075	–998.47	–981
93.22	106.17	–635.50	–654.78	–790.00	–776	40.00	–23	48.25	46.25	–1005.93	–996.33
78.89	138.86	–623.25	–658	–783.17	–761.75	–55.50	–45.11	15.00	23	–984.07	–999.33
18.22	121.14	–638.25	–688	–782.67	–757	–112.00	–20.11	22.00	24	–986.27	–997.67
102.17	113.5	–632.25	–640.22	–781.17	–771.2	4.5	–17	35.17	158.83	–1006.5	8.17
102	114.67	–634.5	–640	–778.83	–788.44	0.5	1.22	28.67	36.33	–1001.25	–990.5
93.33	104.6	–637.75	–618.83	–770.83	–752.5	8.5	–17.89	36.33	36.67	–999.25	–1000.75
104.33	106.33	–625.75	–636.89	–785.67	–775.22	3	–2.22	34	23.67	–1000.75	–996
102	101.5	–633.25	–643.44	–789.67	–760	18.62	–20.33	40.67	13.17	–1007.5	–1004.5
96.00	101.67	–635.75	–646	–800.00	–743.67	20.52	–0.44	28.83	16.83	–1002.00	–1009.75
114.11	131.5	–647.00	–641.56	–784.75	–795.11	18.33	11.11	37.00	51	–1002.27	–1006.25
82.44	92.33	–645.75	–651.11	–801.83	–795.89	–10.83	–4.33	52.75	49	–1000.93	–1001.5
86.00	101.67	–658.00	–673.44	–788.17	–803.22	–10.33	10.11	34.25	48.5	–994.07	–1002.25
86.33	150	–618.25	–669.56	–830.33	–820.67	11.00	–40.33	9.00	36.17	–993.67	–1011.17
94.00	100.29	–642.67	–642.8	–782.17	–783.25	2.00	15.22	23.40	46.5	–1000.00	–998.17
96.67	110.33	–642.25	–648.5	–789.83	–773	13.00	–1.11	30.00	45.17	–996.50	–997.67
97.67	101.33	–650.25	–658.75	–786	–786.5	17.88	–1.44	33.67	38.17	–995.75	–1002.5
127.67	98.56	–651.50	–651	–786.17	–748.5	18.25	7	39.83	39.17	–1001.50	–1003.5
102	80.89	–643	–656.75	–773.67	–749.5	17.88	–12.11	29.5	40	–1007	–996.67
105.5	103.33	–644.75	–636.5	–777.67	–767.75	4.5	22	27.17	38.83	–999.5	–1003.17
90.50	86.33	–648.25	–653.75	–762.17	–761.5	23.00	–37.78	37.00	42.5	–998.25	–992
105.50	56.78	–637.50	–650.25	–789.33	–758	1.25	–5	26.50	47.83	–990.25	–998.17
78.83	61.22	–645.00	–673	–752.50	–764.5	16.75	4.89	38.33	67.17	–999.25	–992
78.33	84.11	–648.285	–648.5	–786.5	–784.75	31.75	–40.33	69.33	23.67	–987.5	–1002.83
0.039		0.033		0.018		0.02		0.21		0.688	

Indexed in: [Current Contents/Clinical Medicine] [SCI Expanded] [ISI Alerting System] [ISI Journals Master List] [Index Medicus/MEDLINE] [EMBASE/Excerpta Medica] [Chemical Abstracts/CAS]

Table 3. Results of consistency analysis between the two observers.

Consistency analysis of the detection and diagnosis of mini-nodules with the size of 5 mm at (–650 HU and –800 HU) by the two radiologists					
		Value	Progressive standard error	Approximate Tb	Approximate significance
Measurement	Kappa	0.929	0.029	15.548	<0.001
The number of effective observations		280			
a. Without false assumptions					
b. Using progressive standard error with false assumptions					
Consistency analysis of the overall image quality by the two radiologists					
		Value	Progressive standard error	Approximate Tb	Approximate significance
Measurement	Kappa	0.819	0.057	11.108	<0.001
Number of effective observations					
a. Without false assumptions					
b. Using progressive standard error with false assumptions					

Table 4. Radiation doses satisfying the screening of nodules (5 mm, –630 HU).

mA / kVp	360	320	280	240	200	160	120	80	40	20
Detection of mini-modules at (5 mm, –630 HU) with fixed tube current by HDCT and ED (mSv)										
80	3.66	3.25	2.84	2.44	2.03	1.63	1.22	0.81	0.41	
100	6.85	6.09	5.33	4.57	3.80	3.04	2.28	1.52	0.76	**0.38**
120	10.87	9.66	8.45	7.25	6.04	4.83	3.62	2.41	1.21	0.60
140	15.51	13.78	12.06	10.34	8.61	6.89	5.17	3.44	1.72	0.86
Detection of small nodules at (5 mm, –630 HU) with fixed tube current by VCT and ED (mSv)										
80	3.62	3.21	2.81	2.41	2	1.6	1.2	0.8	**0.4**	
120	10.75	9.53	8.33	7.14	5.95	4.76	3.57	2.37	1.19	0.59
140	15.24	13.51	11.81	10.13	8.43	6.75	5.06	3.37	1.68	0.84

nodules could be detected via the scanning parameters as follows: 140 kVp and 20 mA, 120 kVp and 20 mA, 100 kVp and 40 mA, along with 80 kVp and 120 mA, and the ED was the lowest (0.60 mSv) at 120 kVp and 20 mA. The detection requirements of all pulmonary nodules could be achieved via scanning parameters that included 140 kVp and 40 mA, 120 kVp and 80 mA, 100 kVp and 120 mA, and 80 kVp and 200 mA, and the ED was the lowest (1.72 mSv) at 140 kVp and 40 mA.

On SDCT, the pulmonary nodules could be detected via the scanning parameters of 140 kVp and 40 mA, 120 kVp and 80 mA, and 80 kVp and 280 mA, and the ED was the lowest (1.68 mSv) at 140 kVp and 40 mA. The detection requirements of all pulmonary nodules could be achieved at 140 kVp and 120 mA and 120 kVp and 200 mA, while the ED was the lowest (5.06 mSv) at 140 kVp and 120 mA (Tables 6, 7 and Figures 6, 7).

Discussion

Worldwide, low-dose computed tomography (LDCT) screening of the lung has become increasingly used. Currently, studies from follow-up data of CT screening for lung cancer have shown that there is a risk of lung cancer for pulmonary nodules <10 mm (usually 4–6 and 6–8 mm) [21,22]. Also, some studies have shown that the detection and diagnosis of lung

Indexed in: [Current Contents/Clinical Medicine] [SCI Expanded] [ISI Alerting System] [ISI Journals Master List] [Index Medicus/MEDLINE] [EMBASE/Excerpta Medica] [Chemical Abstracts/CAS]

Table 5. Radiation doses for diagnosis of small nodules (5 mm, –630 HU).

mA / kVp	360	320	280	240	200	160	120	80	40	20
Diagnosis of mini-nodules (5 mm, –630 HU) with fixed tube current by HDCT and ED (mSv)										
80	3.66	3.25	2.84	2.44	2.03	1.63	1.22	**0.81**		
100	6.85	6.09	5.33	4.57	3.80	3.04	2.28	1.52		
120	10.87	9.66	8.45	7.25	6.04	4.83	3.62	2.41	1.21	
140	15.51	13.78	12.06	10.34	8.61	6.89	5.17	3.44	1.72	0.86
Detection of small nodules at (5 mm, –630 HU) with fixed tube current by VCT and ED (mSv)										
80	3.62	3.21	2.81	2.41	2	1.6	**1.2**			
120	10.75	9.53	8.33	7.14	5.95	4.76	3.57	2.37		
140	15.24	13.51	11.81	10.13	8.43	6.75	5.06	3.37	1.68	

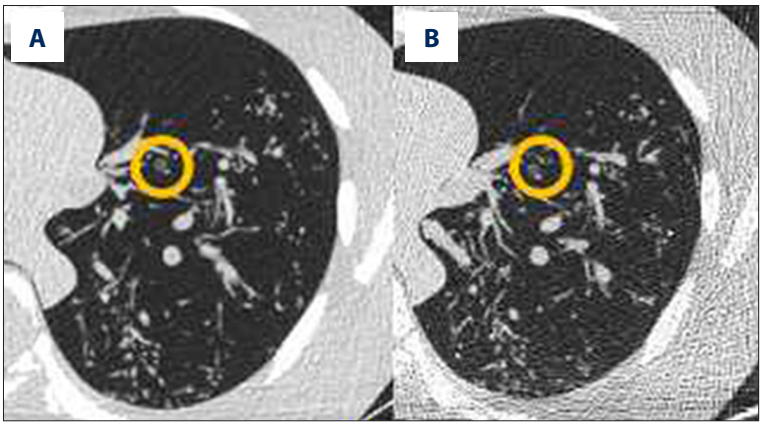

Figure 4. Detection of small lung nodules (5 mm, –630 HU) in the LUNGMAN N1 phantom multipurpose anthropomorphic chest model. The left panel (**A**) is high-definition computed tomography (HDCT) image, using the Discovery HD750 scanner at 100 kVp and 20 mA. The right panel (**B**) is the standard-definition CT (SDCT) image, using the Lightspeed VCT scanner at 80 kVp and 40 mA.

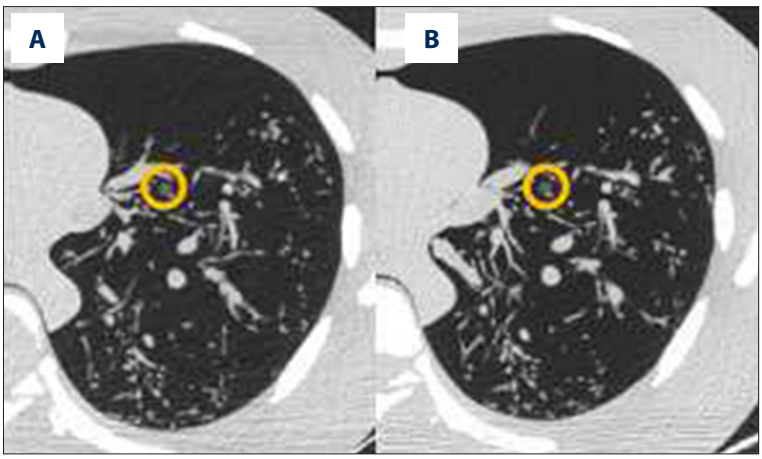

Figure 5. Diagnosis of the small lung nodules (5 mm, –630 HU) in the LUNGMAN N1 phantom multipurpose anthropomorphic chest model. The left panel (**A**) is high-definition computed tomography (HDCT) image using the Discovery HD750 scanner at 80 kVp and 80 mA. The right panel (**B**) is the standard-definition CT (SDCT) image, using the Lightspeed VCT scanner at 80 kVp and 120 mA.

Indexed in: [Current Contents/Clinical Medicine] [SCI Expanded] [ISI Alerting System] [ISI Journals Master List] [Index Medicus/MEDLINE] [EMBASE/Excerpta Medica] [Chemical Abstracts/CAS]

Table 6. Radiation doses for detecting mini-nodules (5 mm, –800 HU).

mA / kVp	360	320	280	240	200	160	120	80	40	20
Detection of mini-nodules (5 mm, –800 HU) with fixed tube current by HDCT and ED (mSv)										
80	3.66	3.25	2.84	2.44	2.03	1.63	1.22			
100	6.85	6.09	5.33	4.57	3.80	3.04	2.28	1.52	0.76	
120	10.87	9.66	8.45	7.25	6.04	4.83	3.62	2.41	1.21	**0.60**
140	15.51	13.78	12.06	10.34	8.61	6.89	5.17	3.44	1.72	0.86
Detection of mini-nodules (5 mm, –800 HU) with fixed tube current by VCT and ED (mSv)										
80	3.62	3.21	2.81							
120	10.75	9.53	8.33	7.14	5.95	4.76	3.57	2.37		
140	15.24	13.51	11.81	10.13	8.43	6.75	5.06	3.37	**1.68**	

Table 7. Radiation doses for diagnosis of detecting small nodules (5 mm, –800 HU).

mA / kVp	360	320	280	240	200	160	120	80	40	20
Diagnosis of mini-nodules (5 mm, –800 HU) with fixed tube current by HDCT and ED (mSv)										
80	3.66	3.25	2.84	2.44	2.03					
100	6.85	6.09	5.33	4.57	3.80	3.04	2.28			
120	10.87	9.66	8.45	7.25	6.04	4.83	3.62	2.41		
140	15.51	13.78	12.06	10.34	8.61	6.89	5.17	3.44	**1.72**	
Diagnosis of mini-nodules (5 mm, –800 HU) with fixed tube current by VCT and ED (mSv)										
80										
120	10.75	9.53	8.33	7.14	5.95					
140	15.24	13.51	11.81	10.13	8.43	6.75	**5.06**			

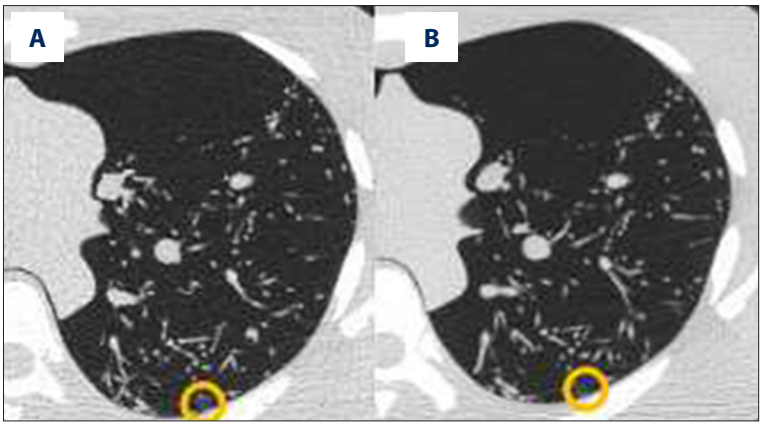

Figure 6. Detection of small lung nodules (5 mm, –800 HU) in the LUNGMAN N1 phantom multipurpose anthropomorphic chest model. The left panel (**A**) is high-definition computed tomography (HDCT) image using the Discovery HD750 scanner at 120 kVp and 20 mA. The right panel (**B**) is the standard-definition CT (SDCT) image, using the Lightspeed VCT scanner at 140 kVp and 40 mA.

Indexed in: [Current Contents/Clinical Medicine] [SCI Expanded] [ISI Alerting System] [ISI Journals Master List] [Index Medicus/MEDLINE] [EMBASE/Excerpta Medica] [Chemical Abstracts/CAS]

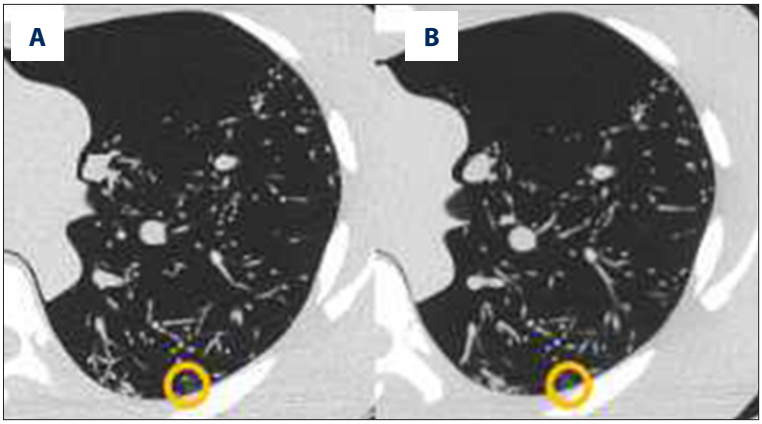

Figure 7. Detection of small lung nodules (5 mm, –800 HU) in the LUNGMAN N1 phantom multipurpose anthropomorphic chest model. The left panel (**A**) is high-definition computed tomography (HDCT) image using the Discovery HD750 scanner at 140k Vp and 40 mA. The right panel (**B**) is the standard-definition CT (SDCT) image, using the Lightspeed VCT scanner at 140 kVp and 120 mA.

cancer on the CT scans have been shown to depend on the experience of the radiologists [3,23–31]. The introduction of artificial intelligence into the detection and diagnosis of small lung nodules can assist in the recording the size, morphology, border, and growth rate. Also, although the lesions of lung cancer are small in the early stage, metastasis may occur, resulting in a reduced 5-year survival even after the treatment. Therefore, the detection of small pulmonary nodules on imaging is important in the detection of early-stage lung cancer.

However, the radiation dose using LDCT is extremely low, which can lead to reduced image quality, reducing the detection and diagnostic sensitivity. Therefore, the reduction of effective radiation dose without losing image quality would be desirable. Attempts to reduce the radiation dose have included altering the scanning parameters (such as milliamperage and peak kilovoltage) and using post-processing reconstruction algorithms. Based on the guidelines of Fleischner Society in 2017, a regular follow-up is not essential for pulmonary nodules found by CT that have no high-risk factors and are <6 mm in size [4]. Therefore, the standard of image quality should able to detect small lung nodules, between 5–6 mm in diameter, while selecting the scanning program.

In this study, various tube currents and voltages were set for high-definition computed tomography (HDCT) and standard-definition CT (SDCT). The ability to detect the spherical pulmonary nodules with different sizes and densities in the LUNGMAN N1 anthropomorphic chest model were objectively evaluated by the investigators to identify the most appropriate scanning conditions. In 2013, the use of the Siemens 64-row CT was reported, and the tube voltages were set to 80, 100, and 120 kVp, while the tube currents were set to 10, 20, 40, 75, and 110 mAs [8]. Pulmonary nodules of 5 mm diameter were identified, but the density of the nodules was not specified [8].

The identification of non-solid nodules is more difficult when compared with solid nodules, which means that if lung cancer screening is performed based on the scanning parameters of solid nodules alone, malignant tumor nodules may be missed. Most early-stage lung adenocarcinomas, including atypical adenomatous hyperplasia (AAH), adenocarcinoma *in-situ* (AIS), and minimally-invasive adenocarcinoma (MIA) do not form solid nodules. In this study, the sizes of the nodules were 5, 8, 10, and 12 mm, which satisfied the threshold recommended in the treatment guidelines of pulmonary nodules by Fleischer Society in 2017 [4]. The CT values of pulmonary nodules were set at –630 HU and –800 HU, which almost satisfied the display requirements for pulmonary nodules with different densities. Furthermore, the CT density should be extended to the non-solid pure ground-glass opacity nodules (GGNs), as the detection and diagnosis of non-solid small GGNs are important in the study of lung cancer. An in-depth investigation of this kind of pulmonary nodule suggests that it is important to detect and treat the lung cancer at the earliest stage, based on the histopathology results obtained from examining the Chinese population with pulmonary nodules. The present study used multiple sets of screening parameters, including a tube voltage of 80–140 kVp and a tube current of 20–360 mA, and the CT scanning conditions were more comprehensive when compared with those in previous studies.

In this study, the use of HDCT resulted in a 5% lower radiation dose, while maintaining comparable image quality for imaging small pulmonary nodules (5–12 mm). This finding is supported by the findings from previously reported studies [32,33]. Previous studies have shown the optimization of low-dose scanning images using an adaptive statistical iterative reconstruction algorithm (ASIR), which compensated for the image quality. In this study, a 40% weighted ASIR was used for HDCT, which is a commonly used default iterative weighting that verified the scope of the scanning conditions. Using the filtered back projection (FBP) algorithm and ASIR has been previously shown to provide convincing results [34–36], which may explain the differences in CT values of pulmonary nodules (5 mm, 100 HU; 5 mm, –630 HU; 5 mm, –800 HU) under same scanning condition between two scanners, which increased when the CT values decreased. The measurements from HDCT were

Indexed in: [Current Contents/Clinical Medicine] [SCI Expanded] [ISI Alerting System] [ISI Journals Master List] [Index Medicus/MEDLINE] [EMBASE/Excerpta Medica] [Chemical Abstracts/CAS]

close to the real CT values of the nodules. When the same low dose scanning protocol was applied, some deviation may occur using earlier versions of the CT scanner or CT scanners without iterative reconstruction.

The results of this study showed that among the detection requirements of the eight small lung nodules used in the anthropomorphic chest model, the scanning conditions were the highest for those with a CT value -800 HU and size 5 mm. This phenomenon indicated that the detection requirements of all other small lung nodules could be achieved if the scanning conditions of these small lung nodules were achieved. Therefore, we recommend 140 kVp and 40 mA in the mode of fixed tube voltage and tube current using HDCT, while 120 kVp and 200 mA were preferable in the mode of fixed tube voltage and tube current on the SDCT in clinical practice.

The present study confirmed the small lung nodules of 5 mm diameter (–630 HU) can be detected at different energy levels (80, 100, 120, and 140 kVp in HDCT; 80, 100, and 120 in SDCT) with 40 mA. The minimum radiation dose was 0.41 mSv. Therefore, it may be speculated that 40 mA was the lowest tube current when the tube voltage was not limited. While observing the details of the small lung nodules with the size of 5 mm and CT value –630 HU, 80 mA was the lowest tube current on HDCT if there was no limitation in tube voltage, while 120 mA was the lowest tube current for SDCT. To detect the pulmonary nodules with 5 mm diameter and –800 HU CT value, 120 mA was the lowest tube current on HDCT, while 280 mA was the lowest tube current on SDCT if there the tube voltage was unlimited. For detecting the pulmonary nodules with the diameter of 5 mm and CT value of –800 HU, 200 mA was the lowest tube current on HDCT if there was no limitation on tube voltage. For SDCT, the detection requirements could not be achieved under all tube currents if the tube voltage was 80 kVp. However, the tube voltage at 120 kVp and/or tube current ≥200 mA could fulfill all the detection requirements.

In the case that other parameters were fixed, the radiation dose on HDCT at 100 kVp and 20 mA was similar to that for SDCT at 80 kVp and 20 mA. However, HDCT with 40% weighted ASIR showed a better image quality than FBP using SDCT Therefore, a low radiation dose could be used for HDCT for pulmonary screening.

This study had several limitations. An average or standard body mass index (BMI) was used to design the LUNGMAN N1 phantom multipurpose anthropomorphic chest model used in this study. The scanning parameters should be adjusted appropriately based on the BMI values of the patients in clinical practice. However, this study investigated the effects of various tube parameters with respect to the display of pulmonary nodules only on SDCT and HDCT. Therefore, scanning parameters should be converted based on the image quality if LDCT screening of the lung is conducted using other devices.

Conclusions

This study used the LUNGMAN N1 phantom multipurpose anthropomorphic chest model with artificial pulmonary nodules (diameter: 5, 8, 10, and 12 mm) and showed that with computed tomography (CT) scanning conditions at 100 kVp and 20 mA, high-definition CT (HDCT) could detect pulmonary nodules with the diameter ≥5 mm and density ≥–630 HU. Compared with the lowest scanning conditions using standard-definition CT (SDCT) the dose decreased by 5%. However, the lowest scanning parameters were 80 kVp and 80 mA on HDCT for detection of the nodules, which decreased by 32.5% when compared with SDCT. The pulmonary nodules with ≥5 mm diameter and ≥–800 HU density could be detected at 120 kVp and 20 mA on HDCT, which reduced the dose by 64.3% when compared with the SDCT. Detection of the nodules could also be performed at 140 kVp and 40 mA by HDCT, which decreased the dose by 66% when compared with the SDCT.

References:

1. Torre LA, Bray F, Siegel RL et al: Global cancer statistics, 2012. Cancer J Clin, 2015; 65: 87–108
2. Koh WJ, Greer BE, Abu-Rustum NR et al: Vulvar Cancer, Version 1.2017, NCCN Clinical Practice Guidelines in Oncology. J Natl Compr Canc Netw, 2017; 15: 92–120
3. Liu Y, Wang H, Li Q et al: Radiologic features of small pulmonary nodules and lung cancer risk in the national lung screening trial: A nested case-control study. Radiology, 2018; 286: 298–306
4. MacMahon H, Naidich DP, Goo JM et al: Guidelines for management of incidental pulmonary nodules detected on CT images: From the Fleischner Society 2017. Radiology, 2017; 284: 228–43
5. Yoshinaga S, Mabuchi K, Sigurdson AJ et al: Cancer risks among radiologists and radiologic technologists: Review of epidemiologic studies. Radiology, 2004; 233: 313–21
6. Berrington DGA, Darby S: Risk of cancer from diagnostic X-rays: Estimates for the UK and 14 other countries. Lancet, 2004; 363: 345–51
7. Cardis E, Vrijheid M, Blettner M et al: The 15-Country Collaborative Study of Cancer Risk among Radiation Workers in the Nuclear Industry: Estimates of radiation-related cancer risks. Radiat Res, 2007; 167: 396–416
8. Botelho MP, Agrawal R, Gonzalez-Guindalini FD et al: Effect of radiation dose and iterative reconstruction on lung lesion conspicuity at MDCT: Does one size fit all? Eur J Radiol, 2013; 82: e726–33
9. Xie X, Willemink MJ, de Jong PA et al: Small irregular pulmonary nodules in low-dose CT: Observer detection sensitivity and volumetry accuracy. Am J Roentgenol, 2014; 202: W202–9
10. Vardhanabhuti V, Pang CL, Tenant S et al: Prospective intra-individual comparison of standard dose versus reduced-dose thoracic CT using hybrid and pure iterative reconstruction in a follow-up cohort of pulmonary nodules-effect of detectability of pulmonary nodules with lowering dose based on nodule size, type, and body mass index. Eur J Radiol, 2017; 91: 130–41
11. Raz DJ, Wu GX, Consunji M et al: The effect of primary care physician knowledge of lung cancer screening guidelines on perceptions and utilization of Low-Dose computed tomography. Clin Lung Cancer, 2018; 19: 51–57

Indexed in: [Current Contents/Clinical Medicine] [SCI Expanded] [ISI Alerting System] [ISI Journals Master List] [Index Medicus/MEDLINE] [EMBASE/Excerpta Medica] [Chemical Abstracts/CAS]

12. Gao F, Li M, Ge X et al: Multi-detector spiral CT study of the relationships between pulmonary ground-glass nodules and blood vessels. Eur Radiol, 2013; 23: 3271–77
13. Gao F, Li M, Sun Y et al: Diagnostic value of contrast-enhanced CT scans in identifying lung adenocarcinomas manifesting as GGNs (ground glass nodules). Medicine, 2017; 96: e7742
14. Zhang Y, Tang J, Xu J et al: Analysis of pulmonary pure ground-glass nodule in enhanced dual energy CT imaging for predicting invasive adenocarcinoma: Comparing with conventional thin-section CT imaging. J Thorac Dis, 2017; 9: 4967–78
15. Ichikawa K, Kobayashi T, Sagawa M et al: A phantom study investigating the relationship between ground-glass opacity visibility and physical detectability index in low-dose chest computed tomography. J Appl Clin Med Phys, 2015; 16: 202–15
16. Liu D, Awai K, Funama Y et al: Identification and characterization of focal ground-glass opacity in the lungs by high-resolution CT using thin-section multidetector helical CT: Experimental study using a chest CT phantom. Radiat Med, 2008; 26: 21–27
17. Tang H, Yu N, Jia Y et al: Assessment of noise reduction potential and image quality improvement of a new generation adaptive statistical iterative reconstruction (ASIR-V) in chest CT. Br J Radiol, 2018; 91: 20170521
18. Kim HG, Chung YE, Lee YH et al: Quantitative analysis of the effect of iterative reconstruction using a phantom: Determining the appropriate blending percentage. Yonsei Med J, 2015; 56: 253–61
19. Brady SL, Moore BM, Yee BS, Kaufman RA: Pediatric CT: Implementation of ASIR for substantial radiation dose reduction while maintaining pre-ASIR image noise. Radiology, 2014; 270: 223–31
20. Vorona GA, Ceschin RC, Clayton BL et al: Reducing abdominal CT radiation dose with the adaptive statistical iterative reconstruction technique in children: A feasibility study. Pediatr Radiol, 2011; 41: 1174–82
21. Walter JE, Heuvelmans MA, de Jong PA et al: Occurrence and lung cancer probability of new solid nodules at incidence screening with low-dose CT: Analysis of data from the randomised, controlled NELSON trial. Lancet Oncol, 2016; 17: 907–16
22. Pinsky PF, Gierada DS, Nath PH, Munden R: Lung cancer risk associated with new solid nodules in the national lung screening trial. Am J Roentgenol, 2017; 209: 1009–14
23. Goldstraw P, Chansky K, Crowley J et al: The IASLC lung cancer staging project: Proposals for revision of the TNM stage groupings in the forthcoming (Eighth) edition of the TNM classification for lung cancer. J Thorac Oncol, 2016; 11: 39–51
24. Wakeam E, Acuna SA, Leighl NB et al: Surgery versus chemotherapy and radiotherapy for early and locally advanced small cell lung cancer: A Propensity-Matched analysis of survival. Lung Cancer, 2017; 109: 78–88
25. Bartholmai BJ, Koo CW, Johnson GB et al: Pulmonary nodule characterization, including computer analysis and quantitative features. J Thorac Imaging, 2015; 30: 139–56
26. Raman SP, Schroeder JL, Huang P et al: Preliminary data using computed tomography texture analysis for the classification of hypervascular liver lesions: Generation of a predictive model on the basis of quantitative spatial frequency measurements – a work in progress. J Comput Assist Tomogr, 2015; 39: 383–95
27. Depeursinge A, Yanagawa M, Leung AN, Rubin DL: Predicting adenocarcinoma recurrence using computational texture models of nodule components in lung CT. Med Phys, 2015; 42: 2054–63
28. Aerts HJ, Velazquez ER, Leijenaar RT et al: Decoding tumor phenotype by noninvasive imaging using a quantitative radiomics approach. Nat Commun, 2014; 5: 4006
29. El-Baz A, Beache GM, Gimel'Farb G et al: Computer-aided diagnosis systems for lung cancer: Challenges and methodologies. Int J Biomed Imaging, 2013; 2013: 942353
30. Huang P, Park S, Yan R et al: Added value of computer-aided CT image features for early lung cancer diagnosis with small pulmonary nodules: A matched case-control study. Radiology, 2018; 286: 286–95
31. Cirujeda P, Dicente CY, Muller H et al: A 3-D Riesz-Covariance texture model for prediction of nodule recurrence in lung CT. IEEE Trans Med Imaging, 2016; 35: 2620–30
32. Tanami Y, Jinzaki M, Yamada M et al: Improvement of in-stent lumen measurement accuracy with new high-definition CT in a phantom model: Comparison with conventional 64-detector row CT. Int J Cardiovasc Imaging, 2012; 28: 337–42
33. Yang WJ, Zhang H, Xiao H et al: High-definition computed tomography for coronary artery stents imaging compared with standard-definition 64-row multidectector computed tomography: An initial *in vivo* study. J Comput Assist Tomogr, 2012; 36: 295–300
34. Mueck FG, Michael L, Deak Z et al: Upgrade to iterative image reconstruction (IR) in MDCT imaging: A clinical study for detailed parameter optimization beyond vendor recommendations using the adaptive statistical iterative reconstruction environment (ASIR) Part 2: The chest. Rofo, 2013; 185: 644–54
35. Yamada Y, Jinzaki M, Hosokawa T et al: Dose reduction in chest CT: Comparison of the adaptive iterative dose reduction 3D, adaptive iterative dose reduction, and filtered back projection reconstruction techniques. Eur J Radiol, 2012; 81: 4185–95
36. Huber A, Landau J, Ebner L et al: Performance of ultralow-dose CT with iterative reconstruction in lung cancer screening: Limiting radiation exposure to the equivalent of conventional chest X-ray imaging. Eur Radiol, 2016; 26: 3643–52

Indexed in: [Current Contents/Clinical Medicine] [SCI Expanded] [ISI Alerting System] [ISI Journals Master List] [Index Medicus/MEDLINE] [EMBASE/Excerpta Medica] [Chemical Abstracts/CAS]